Excited states in ^{99}Pd

S. Sihotra,[1] Z. Naik,[2] S. Kumar,[1] K. Singh,[1] J. Goswamy,[1] N. Singh,[1] R. Kumar,[3] R. P. Singh,[3] S. Muralithar,[3] R. K. Bhowmik,[3] R. Palit,[4] and D. Mehta[1,*]

[1]*Department of Physics, Panjab University, Chandigarh 160014, India*

[2]*Department of Physics, Sambalpur University, Sambalpur 143005, India*

[3]*Inter-University Accelerator Centre, New Delhi 110067, India*

[4]*Department of Nuclear and Atomic Physics, Tata Institute of Fundamental Research, Mumbai 400005, India*

(Received 11 October 2010; published 22 February 2011)

Excited states in the ^{99}Pd nucleus populated in the ^{75}As(^{28}Si, p3n) fusion-evaporation reaction at $E_{\rm lab}$ = 120 MeV have been investigated through in-beam γ-ray spectroscopic techniques using an array of Compton-suppressed clover detectors. The level scheme is established up to excitation energy $\sim$11.5 MeV and spin $\sim 25\hbar$ with the addition of about 60 new transitions. The level structures observed in ^{99}Pd have been interpreted in the framework of a microscopic theory based on the deformed Hartree-Fock and angular momentum projection techniques. Band structures at lower spins are based on the low-Ω $\nu g_{7/2}$ and $\nu d_{5/2}$ orbitals, and those at higher spins are reproduced for the $\pi(g_{9/2})^5 \otimes \pi(g_{7/2}) \otimes \nu(g_{7/2})^2 \otimes \nu(h_{11/2})^2 \otimes \nu(g_{9/2})^{-1}$ and $\pi(g_{9/2})^6 \otimes \nu(g_{9/2})^{10} \otimes \nu(g_{7/2})^2 \otimes \nu(h_{11/2})$ configurations. The octupole correlations in ^{99}Pd have been inferred from new interband $E1$ transitions linking the $\Delta I = 1$ states of the bands based on the $\nu h_{11/2}$ and $\nu d_{5/2}$ orbitals ($\Delta l = 3$, $\Delta j = 3$, and $\Delta\pi = -1$) with the deduced $B(E1)$ values $\sim 10^{-6}$ W.u.

DOI: 10.1103/PhysRevC.83.024313 PACS number(s): 23.20.En, 27.60.+j, 21.60.Jz, 25.70.−z

I. INTRODUCTION

The nuclei approaching the neutron and proton major shell closures at $N = Z = 50$ provide a unique opportunity to study the interplay between the single-particle and collective degrees of freedom and the influence of the valence orbitals on deformation. Various new deformation-generating mechanisms have been identified in theoretical interpretation of the observed band structures [1]. Investigations have revealed diversity in band structures resulting from coupling of the $g_{9/2}$, $d_{5/2}$, $g_{7/2}$, and $h_{11/2}$ valence nucleons and the core-excited configurations. The proton particle-hole excitations across the major shell gap are energetically possible due to the strong proton-pair correlations and proton-neutron interaction between the spin-orbit partner orbitals [2]. For the nuclei approaching $Z = 50$ from below, the proton Fermi surface lies near the oblate-driving high-Ω orbitals of the intruder $\pi g_{9/2}$ subshell. Strongly prolate-driving low-Ω $\nu h_{11/2}$ subshell orbitals are accessible at low excitation energies for the nuclei receding the $N = 50$ shell closure. The delicate interplay of strongly shape-driving $\pi g_{9/2}$ and $\nu h_{11/2}$ orbitals can influence the overall shape of the nucleus and result in γ-soft (triaxial) shapes with modest deformation (ϵ_2) $\approx$ 0.15 [3,4]. The relevant intriguing triaxiality based phenomena such as magnetic rotation [5,6] and degenerate twin bands [7–10] have been reported in this mass region. The twin degenerate dipole bands with similar energy staggering and electromagnetic strengths have been explained with aplanar tilted rotation of the triaxial core along with the valence neutrons and protons aligned along the two extreme axes of the core. The truncated shell model calculations prescribe an alternative angular momentum coupling scheme, namely, the chopstick model [11], to explain these bands.

Specific noncollective "aligned" states with the nuclear spin made up completely from angular momentum contributions of the particles and holes in open shells, are able to compete energetically with weakly deformed collective structures in the vicinity of the $Z = 50$ shell closure. The maximally aligned states have been observed in the ^{98,99}Ag [12,13] and ^{98,102,103}Pd [14–16] isotopes. In ^{102}Pd [15], four band structures have been observed up to termination and interpreted in terms of valence-space and core-excited configurations. Terminating configurations have also been identified in various isotopes of $_{52}$Te [17] and $_{53}$I [18]. For the nuclei in this mass region, the negative-parity $h_{11/2}$ intruder and the normal parity $d_{5/2}$ neutron-proton orbitals with $\Delta l = 3$, $\Delta j = 3$, and $\Delta\pi = -1$ are near the Fermi surface. Interaction between such orbitals is expected to result in octupole correlations. Indeed, octupole collectivity has been observed in the $_{54}$Xe [19–22], $_{55}$Cs [23–26], and $_{56}$Ba [27,28] isotopes.

The present work reports in-beam γ-ray spectroscopic investigations of band structures in the ^{99}Pd nucleus and their microscopic description using the deformed Hartree-Fock and angular-momentum projection calculations. Low-lying levels of ^{99}Pd have been investigated from the EC-β^+ decay of ^{99}Ag by Huyse *et al.* [29]. Piel and Goldhaber [30] studied the excited states in ^{99}Pd through the ^{91}Zr(^{12}C, $4n$) and ^{70}Ge(^{32}S, $2pn$) reactions. Dubuc *et al.* [31] investigated the same through the ^{96}Ru(α, n) and ^{96}Ru(^{6}Li, $p2n$) reactions. These investigations were performed using a few Ge detectors without the Compton suppression. The level scheme of ^{99}Pd reported from the previous experiments is limited with the highest observed state at excitation energy $\sim$4 MeV and spin $\sim 14\hbar$. The existing experimental data do not exhibit any

*dmehta@pu.ac.in

nonyrast negative-parity band built on the $\nu h_{11/2}$ intruder orbital. It is of interest to investigate level structure of the ^{99}Pd nucleus using an advanced array of Compton-suppressed clover detectors [32] and explore the aforementioned features.

II. EXPERIMENTAL DETAILS

Excited states in the ^{99}Pd nucleus were populated in the ^{75}As(^{28}Si, $p3n$) fusion-evaporation reaction at $E_{\rm lab} =$ 120 MeV. The deexcitations were investigated through in-beam γ-ray spectroscopic techniques. The ^{28}Si beam was delivered by the 15UD Pelletron accelerator at Inter University Accelerator Centre (IUAC), New Delhi. The ^{75}As target of thickness 3 mg/cm^2 was prepared by vacuum evaporation and rolled onto a 10 mg/cm^2 thick Pb backing. The recoiling nuclei in the excited states were stopped within the target and the deexciting γ-rays were detected using the Indian National Gamma Array (INGA) consisting of 18 clover detectors mounted in five-rings configuration [32]. The photopeak efficiency of the array is $\sim$3% at the 1.3 MeV γ-ray energy. The clover detectors facilitate coincidence polarization measurements for the γ rays. These detectors used in addback mode result in higher efficiency at γ-ray energies above 1 MeV, which makes the array suitable for the single-particle deexcitations studies near the shell closure. A total of about 300×10^6 triple or higher-fold coincidence events were recorded in the experiment. The data were sorted off-line using the INGASORT program [32] to generate E_γ-E_γ matrices and E_γ-E_γ-E_γ cubes with different conditions. The energy and efficiency calibrations of the clover detectors were done using the ^{133}Ba and ^{152}Eu radioactive sources. The data analysis was performed using the RADWARE analysis package [33] to establish coincidence relationships for various γ transitions. The level scheme of ^{99}Pd developed in the present work is shown in Fig. 1. Relative intensities of γ rays in ^{99}Pd have been extracted from the singles γ spectra and the γ-γ coincidence spectra. The γ-ray intensities normalized with respect to the 264.2 keV ($\frac{7}{2}^+ \rightarrow \frac{5}{2}^+$) transition are listed in Table I.

The directional correlation of oriented states (DCO) ratio analysis [34] has been used to distinguish between dipole and quadrupole transitions. Two-dimensional angular correlation matrices between the detectors at 90° and those at 32° and 148° were constructed. Intensities of coincident transitions were obtained from the the correlation matrices by setting gates on the known low-lying stretched electric quadrupole transitions, viz., 805.7 keV ($11/2^+ \rightarrow 7/2^+$), 881.7 keV ($19/2^+ \rightarrow 15/2^+$), and 832.1 keV ($9/2^+ \rightarrow 5/2^+$), and were used to deduce DCO ratios. The DCO ratios for various transitions in ^{99}Pd obtained from the present work are also listed in Table I. For the INGA geometry, the expected values of DCO ratio are typically $\geqslant$1.0 for the quadrupole transitions and $\leqslant$0.6 for the dipole transitions. The clover detector at 90° was used as a Compton polarimeter to determine the electric or magnetic nature of the γ rays [35]. The integrated polarization directional correlation from oriented nuclei (IPDCO) analysis was done using two asymmetric polarization matrices corresponding to the parallel and perpendicular segments of the clover detector chosen as a Compton polarimeter (with respect to the emission plane) along one axis and the coincident γ rays in all the detectors along the other axis. Further details of the IPDCO analysis relevant to the INGA setup are given elsewhere [34]. The values of the polarization asymmetry parameter obtained from the present measurements are listed in Table I.

III. RESULTS

The present level scheme of ^{99}Pd (Fig. 1) built on the $I^\pi = 5/2^+$ ground state has been established up to $\sim$11.5 MeV excitation energy and $\sim 25\hbar$ spin. It is a significant extension with about 60 new transitions added to the level schemes reported by Piel and Goldhaber [30], and Dubuc *et al.* [31]. Five bands labeled B1–B5 are identified in the level scheme. The present level scheme preserves major features of the earlier reported level schemes mainly consisting of bands B1 and B2 identified to be based on $\nu g_{7/2}$ and $\nu d_{5/2}$, respectively. New negative-parity band B3 and positive-parity band B4 based on the earlier observed $11/2^-$ and $19/2^+$ states [31], respectively, are established. The relevant coincidence spectra in support of the present level scheme of ^{99}Pd are depicted in Figs. 2–5. Multipolarities of the interband and intraband transitions inferred from the present measured DCO and IPDCO ratios have been used for spin-parity assignments to various states. Further it is assumed that the γ transitions bearing major part of the deexcitation intensity in the level scheme are stretched ones.

Band B1 built on the $\nu g_{7/2}$ orbital is the most intensely populated band in ^{99}Pd and band B2 based on the $\nu d_{5/2}$ orbital is the next intensely populated one (Fig. 1). In the neighboring ^{97}Pd [36] and ^{101}Pd [37] isotopes, the $\nu d_{5/2}$ band is the most intensely populated band. Higher excited positive-parity and negative-parity bands in ^{99}Pd decay into states of bands B1 and B2. A new cascade 771.9–213.2 keV of the $E2$ transitions is placed above the $13/2^+$ level in the B2 ($\nu d_{5/2}$) band. The band B5 built on the $I^\pi = 7/2^+$ level at 815 keV has been extended up to the $I^\pi = (15/2^+)$ level at 2194 keV. This band decays to the states of band B1 ($\nu g_{7/2}$) through the 397.0- and 475.0-keV $\Delta I = 1$ transitions and the 1203.0- and 1122.0-keV $\Delta I = 2$ transitions. It also decays to the states of the band B2 ($\nu d_{5/2}$) through the 544-, 636.2-, and 815.2-keV $\Delta I = 1$ transitions. The γ-ray coincidence relationships in the earlier reported [31] portion of the level scheme labeled as B5′ could be confirmed in the present work. The earlier observed $9/2^+$ level at 1540 keV [31] could not be confirmed due to the presence of intense γ rays from other populated nuclei.

In the earlier established level scheme by Piel and Goldhaber [30], a cascade of intense 264.2-, 805.7-, 648.7-, 881.7-, 911.4-, and 493.2-keV transitions is preceded by a 35-keV transition. The present coincidence data confirm the cascade except for placement of the 35-keV transition. This low-energy transition is not reported in the later work by Dubuc *et al.* [31]. In the present work, this transition is not observed but its placement as $21/2^+ \rightarrow 19/2^+$ above the 881.7-keV ($19/2^+ \rightarrow 15/2^+$) transition is confirmed by the energy-sum and coincidence relationships. Various spectra relevant to this part of the level scheme are shown in Figs. 4 and 5(a)–5(f).

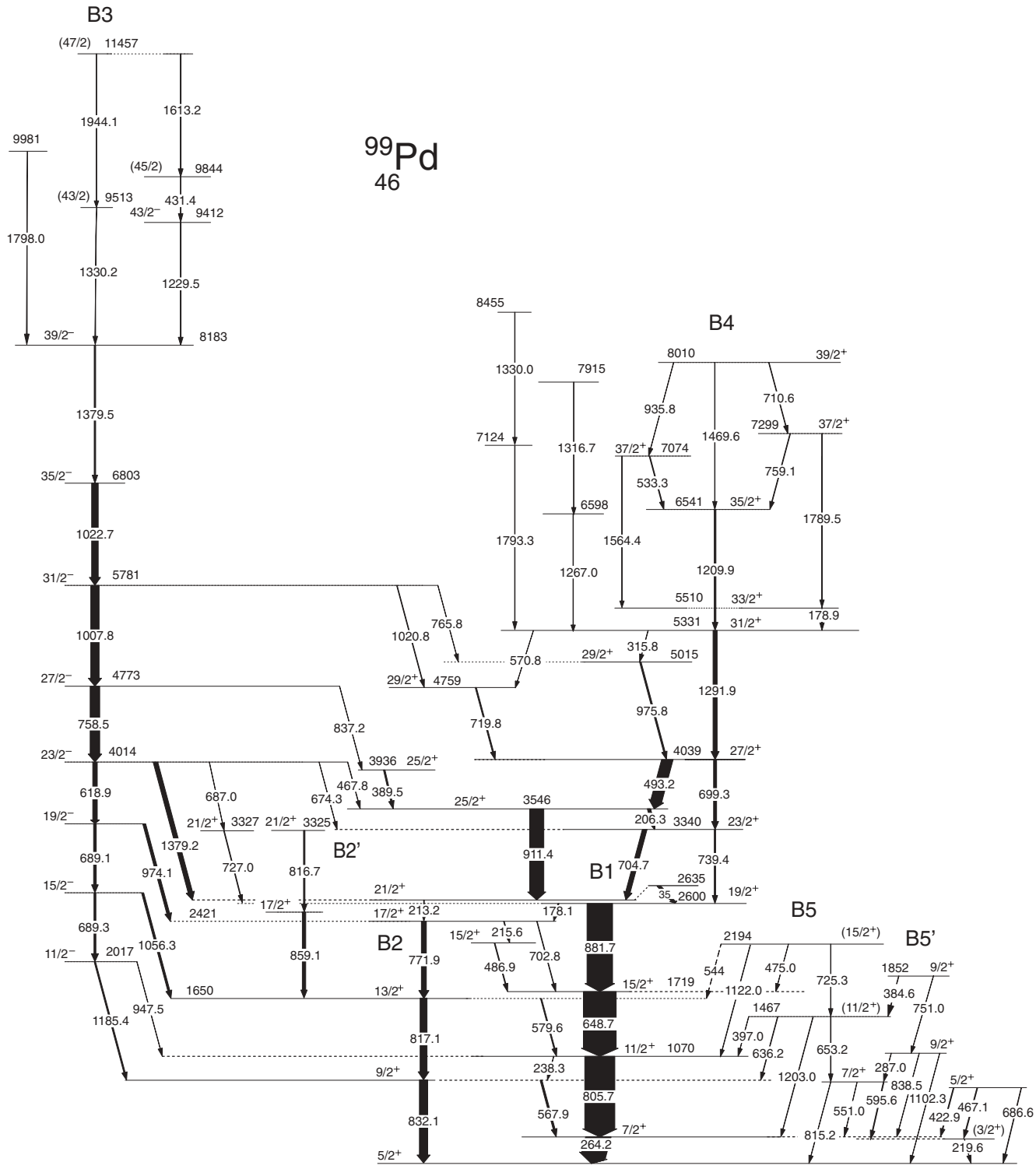

FIG. 1. The level scheme of ^{99}Pd obtained from the present work.

TABLE I. γ-ray transition energies (E_γ), deexciting level energies (E_i), relative intensities (I_γ), and DCO and IPDCO ratios for transitions in ^{99}Pd. The DCO ratios are obtained from the gated spectra on the stretched $E2$ transitions, as mentioned in the text. The uncertainty in energies of intense γ rays is 0.3 keV and that of weak γ rays is up to 0.7 keV.

E_γ (keV)	E_i (keV)	I_γ	J_i^π	→	J_f^π	DCO	IPDCO
35	2635		$21/2^+$	→	$19/2^+$		
178.1	2600	17(3)	$19/2^+$	→	$17/2^+$	0.65(7)	
178.9	5510	8(1)	$33/2^+$	→	$31/2^+$		
206.3	3546	64(6)	$25/2^+$	→	$23/2^+$	0.63(7)	
213.2	2635	21(2)	$21/2^+$	→	$17/2^+$	0.86(3)	
215.6	2421	22(2)	$17/2^+$	→	$15/2^+$		
219.6	220		$(3/2^+)$	→	$5/2^+$		
238.3	1070	4.2(7)	$11/2^+$	→	$9/2^+$	0.59(6)	
264.2	264	1000(50)	$7/2^+$	→	$5/2^+$	0.57(4)	
287.0	1102		$9/2^+$	→	$7/2^+$		
315.8	5331	12(1)	$31/2^+$	→	$29/2^+$	0.45(8)	
384.6	1852		$9/2^+$	→	$(11/2^+)$		
389.5	3936	32(3)	$25/2^+$	→	$25/2^+$	0.53(7)	
397.0	1467	5(1)	$(11/2^+)$	→	$11/2^+$		
422.9	686		$5/2^+$	→	$7/2^+$		
431.4	9844	8(1)	$(45/2)$	→	$43/2^-$		
467.1	686		$5/2^+$	→	$(3/2^+)$		
467.8	4014	13(1)	$23/2^-$	→	$25/2^+$		
475.0	2194	4(1)	$(15/2^+)$	→	$15/2^+$		
486.9	2205	29(2)	$15/2^+$	→	$15/2^+$		
493.2	4039	414(25)	$27/2^+$	→	$25/2^+$	0.58(5)	−0.04(3)
533.3	7074	26(2)	$37/2^+$	→	$35/2^+$	0.51(10)	
544	2194		$(15/2^+)$	→	$13/2^+$		
551.0	815		$7/2^+$	→	$7/2^+$		
567.9	832	75(4)	$9/2^+$	→	$7/2^+$		
570.8	5331	20(5)	$31/2^+$	→	$29/2^+$		
579.6	1650	32(3)	$13/2^+$	→	$11/2^+$		
595.6	815		$7/2^+$	→	$(3/2^+)$		
618.9	4014	134(9)	$23/2^-$	→	$19/2^-$	0.86(2)	0.10(3)
636.2	1467		$(11/2^+)$	→	$9/2^+$		
648.7	1719	930(50)	$15/2^+$	→	$11/2^+$	0.93(8)	0.012(4)
653.2	1467		$(11/2^+)$	→	$7/2^+$		
674.3	4014	10(1)	$23/2^-$	→	$23/2^+$		
686.6	686		$5/2^+$	→	$5/2^+$		
687.0	4014	7(1)	$23/2^-$	→	$21/2^+$		
689.1	3395	75(6)	$19/2^-$	→	$15/2^-$	1.10(8)[a]	
689.3	2706	48(4)	$15/2^-$	→	$11/2^-$		
699.3	4039	43(3)	$27/2^+$	→	$23/2^+$	1.12(15)	
702.8	2421	18(2)	$17/2^+$	→	$15/2^+$		
704.7	3340	184(12)	$23/2^+$	→	$21/2^+$	0.65(12)	
710.6	8010	58(8)	$39/2^+$	→	$37/2^+$	0.45(8)	
719.8	4759	35(4)	$29/2^+$	→	$27/2^+$	0.49(8)	
725.3	2194		$(15/2^+)$	→	$(11/2^+)$		
727.0	3327	23(2)	$21/2^+$	→	$19/2^+$		
739.4	3340	52(4)	$23/2^+$	→	$19/2^+$	0.92(12)	
751.0	1852		$9/2^+$	→	$9/2^+$		
758.5	4773	302(18)	$27/2^-$	→	$23/2^-$	0.89(10)	0.010(4)
759.1	7299	60(5)	$37/2^+$	→	$35/2^+$		
765.8	5781	4(1)	$31/2^-$	→	$29/2^+$	0.57(12)	
771.9	2421	167(15)	$17/2^+$	→	$13/2^+$		
805.7	1070	943(60)	$11/2^+$	→	$7/2^+$	0.98(7)	0.04(1)
815.2	815		$7/2^+$	→	$5/2^+$		
816.7	3325	42(5)	$21/2^+$	→	$17/2^+$		
817.1	1650	215(14)	$13/2^+$	→	$9/2^+$	0.92(10)	

TABLE I. (*Continued.*)

E_γ (keV)	E_i (keV)	I_γ	J_i^π	→	J_f^π	DCO	IPDCO
832.1	832	278(17)	$9/2^+$	→	$5/2^+$		
837.2	4773	9(1)	$27/2^-$	→	$25/2^+$		
838.5	1102		$9/2^+$	→	$7/2^+$		
859.1	2509	70(8)	$17/2^+$	→	$13/2^+$	0.98(11)	
881.7	2600	774(40)	$19/2^+$	→	$15/2^+$	0.98(9)	0.10(4)
911.4	3546	464(30)	$25/2^+$	→	$21/2^+$	0.92(9)	0.04(1)
935.8	8010	25(2)	$39/2^+$	→	$37/2^+$		
947.5	2017	15(1)	$11/2^-$	→	$11/2^+$		
974.1	3395	118(8)	$19/2^-$	→	$17/2^+$	0.67(9)	0.03(1)
975.8	5015	47(5)	$29/2^+$	→	$27/2^+$	0.61(7)	
1007.8	5781	290(20)	$31/2^-$	→	$27/2^-$	1.1(3)	0.03(1)
1020.8	5781	21(2)	$31/2^-$	→	$29/2^+$		
1022.7	6803	264(15)	$35/2^-$	→	$31/2^-$	0.85(10)	
1056.3	2706	55(6)	$15/2^-$	→	$13/2^+$	0.70(9)	0.08(3)
1102.3	1102		$9/2^+$	→	$5/2^+$		
1122.0	2194		$(15/2^+)$	→	$11/2^+$		
1185.4	2017	49(4)	$11/2^-$	→	$9/2^+$		
1203.0	1467		$11/2^+$	→	$7/2^+$		
1209.9	6541	61(5)	$35/2^+$	→	$31/2^+$	0.97(11)	
1229.5	9412	26(2)	$43/2^-$	→	$39/2^-$	0.82(15)	
1267.0	6598	21(3)					
1291.9	5331	146(12)	$31/2^+$	→	$27/2^+$	0.85(9)	
1316.7	7915	7(1)					
1330.0	8455	8(2)					
1330.2	9513	13(2)	(43/2)	→	$39/2^-$		
1379.2	4014	150(12)	$23/2^-$	→	$21/2^+$	0.57(14)[a]	0.11(4)[a]
1379.5	8183	48(5)	$39/2^-$	→	$35/2^-$		
1469.6	8010	15(1)	$39/2^+$	→	$35/2^+$		
1564.4	7074	5(1)	$37/2^+$	→	$33/2^+$		
1613.2	11457	1.5(4)	(47/2)	→	(45/2)		
1789.5	7299	10(2)	$37/2^+$	→	$33/2^+$		
1793.3	7124	10(2)					
1798.0	9981	4(1)		→	$33/2^+$		
1944.1	11457	1.8(7)	(47/2)	→	(43/2)		

[a]The DCO/IPDCO ratio value includes contribution of the next transition in the column.

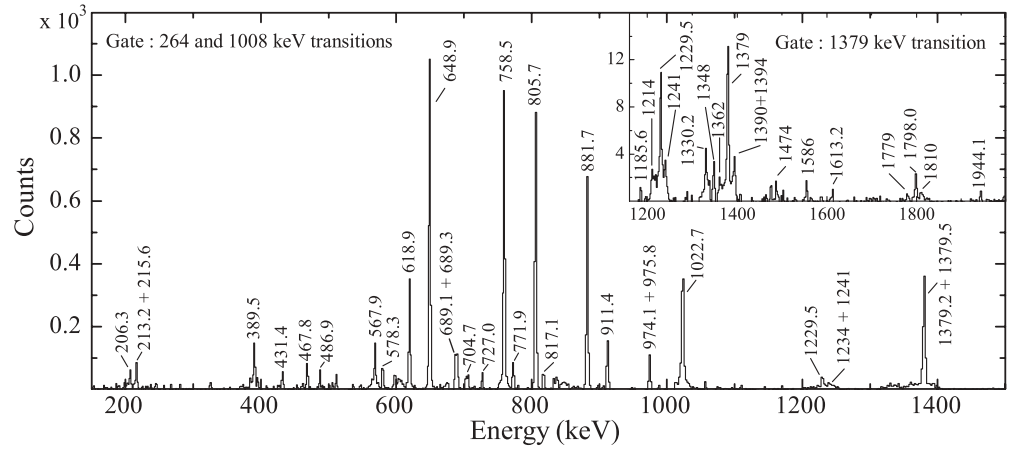

FIG. 2. γ-ray coincidence spectrum with double gate on the 264-keV ($7/2^+ \rightarrow 5/2^+$) and 1008-keV ($31/2^- \rightarrow 27/2^-$) transitions. Inset shows the high energy part of the coincidence spectrum with single gate on the 1379-keV [($39/2^- \rightarrow 35/2^-$) and ($23/2^- \rightarrow 21/2^+$)] transitions. The unmarked peaks are contaminations.

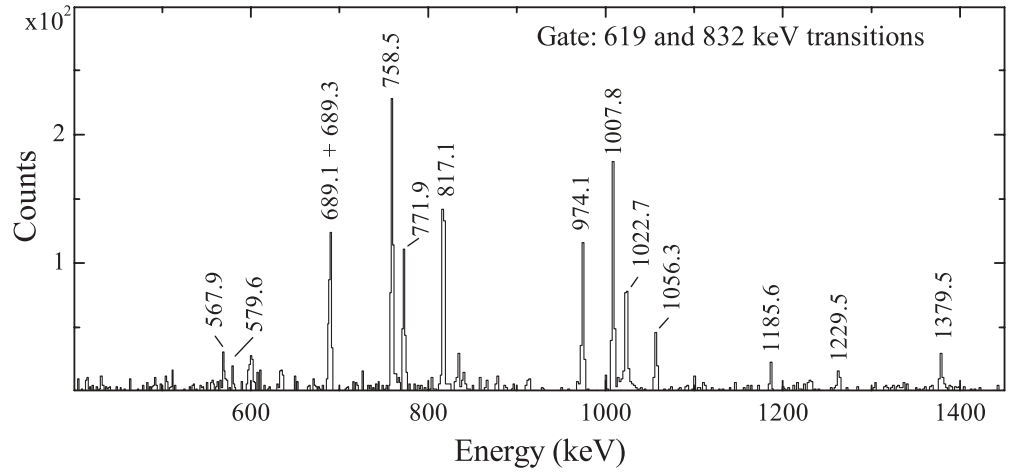

FIG. 3. γ-ray coincidence spectrum with double gate on the 619-keV ($23/2^- \rightarrow 19/2^-$) and 832-keV ($9/2^+ \rightarrow 5/2^+$) transitions. The unmarked peaks are contaminations.

Spectra shown in Figs. 5(a)–5(d) confirm that (i) the 704.7-, 739.4-, and 911.4-keV transitions are parallel, and (ii) the 206.3- and 699.3-keV transitions are in coincidence with the 704.7-, 739.4-, and 881.7-keV transitions and parallel to the 911.4-keV transition, and (iii) the 493.2-keV transition is in coincidence with the 206.3-keV transition and parallel to the 699.3-keV transition. Further, the γ-ray intensity pattern obtained from the spectra shown in Figs. 5(a) and 5(b) indicate that the 704.7- and 739.4-keV transitions feed or depopulate the same level. Figures 5(a)–5(e) support that the parallel-lying 213.2- and 178.1-keV transitions are in coincidence with the 771.9- and 911.4-keV transitions, and parallel to the 881.7-keV transition. The 215.6-to-486.9-keV cascade is in coincidence with the 911.4-to-213.2-keV cascade and parallel to the 771.9- and 881.7-keV transitions [Figs. 5(a)–5(f)]. These observations confirm placement of the 213.2-, 739.4-, and 699.3-keV transitions as crossover to the 178.1-to-35-, 704.7-to-35-, and 493.2-to-206.3-keV cascades, respectively. The intensity balance at the 2635-keV state depopulated by the 35-keV transition does not indicate any isomeric state with a lifetime that could be inferred in the present coincidence set up with time window $(2\tau) = 200$ ns. It favors dipole nature for the 35-keV transition with $\Delta I = 0$ or 1. The 35-keV transition is assigned $21/2^+ \rightarrow 19/2^+$ on the basis of the level spins inferred from the assigned multipolarity of the neighboring transitions. The present DCO and IPDCO values suggest the 493.2-, 881.7-, and 911.4-keV transitions to be $M1$, $E2$, and $E2$, respectively. The 35-keV transition is also inferred to be magnetic dipole by Piel and Goldhaber [30].

The positive-parity band B4 with the lowest observed level at 2600 keV with $I^\pi = 19/2^+$ is established up to 8010-keV level with $I^\pi = 39/2^+$. The lower inband 739.4- and 699.3-keV transitions are weak as band B4 decays out through intense 493.2-keV ($27/2^+ \rightarrow 25/2^+$) and 704.7-keV ($23/2^+ \rightarrow 21/2^+$) $M1$ transitions. The level structure above the $31/2^+$ state at 5331 keV is complex and the γ-ray intensity is fragmented. Weak high-energy transitions placed in the upper part of band B4 are shown in the spectrum with double gate on the 493- and 1292-keV transitions (inset of Fig. 4).

The negative-parity band B3 comprises mainly of the $\Delta I = 2$ quadrupole transitions and is built on the previously observed $I^\pi = 11/2^-$ level at 2017 keV. It is established up to the $I^\pi = (47/2^-)$ level in the present work. Various new transitions in this band are shown in Fig. 2. In this band, the γ-ray intensity is higher above the 4014-keV level. The $23/2^+$ or $25/2^+$ spin-parity for the 4014-keV level is also not favored as it leads to the $M2$ or $E3$ multipolarity for the 618.9-keV transition, which is not likely. Also, the present DCO and IPDCO values favor $E2$ multipolarity for the 618.9-keV transition. The $11/2^-$, $15/2^-$, $19/2^-$, and $23/2^-$states in band B3 decay into the $9/2^+$, $13/2^+$, $17/2^+$, and $21/2^+$ states, respectively, of band B2. The DCO and IPDCO ratios for the interband 1056.3-, 974.1-, and 1379.2-keV, $\Delta I = 1$ transitions support the electric dipole character. The measured ratios for the 1379.2-keV transition includes contribution of weak 1379.5-keV ($39/2^- \rightarrow 35/2^-$) transition in band B3. The intensity of the competing 1056.3-, 974.1-, and 1379.2-keV interband $E1$ transitions is comparable to the corresponding intraband $E2$ transitions. The $11/2^-$ bandhead also decays to the $11/2^+$ state of band B1 ($\nu g_{7/2}$) through weak 947.5-keV transition. The $23/2^-$, $27/2^-$, and $31/2^-$ states decay to the $19/2^+$, $25/2^+$, and $27/2^+$ states through the 687.0-to-727.0-keV cascade, 837.2-to-389.5-keV cascade, and a parallel pair of 1020.8-to-719.8-keV and 765.8-to-975.8-keV cascades, respectively. The intermediate levels in the cascades at 3327, 3936, and 4759 keV are assigned $21/2^+$, $25/2^+$, and $29/2^+$, respectively. Negative parity is not expected as these levels lie lower than the corresponding negative-parity $I - 1$ states in intensely populated band B3.

The structure above the $I^\pi = 39/2^-$ level at 8183 keV is complex and high energy transitions of 1214, 1234, 1241, 1348, 1362, 1394, 1474, 1586, 1779, and 1810 keV are observed in coincidence with the 1379-keV (inset of Fig. 2) and the other transitions in band B3. However, their placement could not be confirmed. The parallel lying 1229.5-431.4-1613.2 keV and 1330.2-to-1944.1-keV γ-transition cascades result in the uppermost levels with the same 11457-keV energy. However, it is not possible to rule out if these

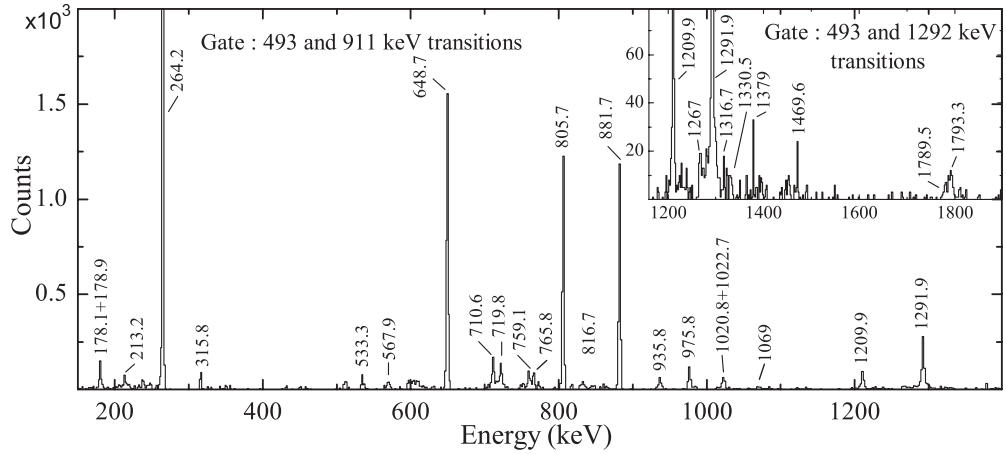

FIG. 4. γ-ray coincidence spectrum with double gate on the 493-keV ($27/2^+ \rightarrow 25/2^+$) and 911-keV ($25/2^+ \rightarrow 21/2^+$) transitions. Inset shows the high energy part of the coincidence spectrum with double gate on the 493- and 1292-keV ($31/2^+ \rightarrow 27/2^+$) transitions. The unmarked peaks are contaminations.

are distinct. The placement of the 1007.8-keV transition as $31/2^- \rightarrow 27/2^-$ (Fig. 1) is confirmed on the basis of γ-ray energy-sum, coincidence, and intensity relationships. It was placed above the 911.4-keV transition and parallel to the 493.2-keV transition in the earlier work [31].

IV. DISCUSSION

For odd-A nuclei in the near shell-closure mass region, low-excitation bands are relatively easier to identify because of the limited possible shell-model configurations. In case of ^{99}Pd ($Z = 46$, $N = 53$), there are four proton holes in the $g_{9/2}$ orbital and three neutrons outside the $N = 50$ shell closures. The level scheme at lower angular momentum consists of B1 and B2 bands, which are based on single-particle $\nu g_{7/2}$ and $\nu d_{5/2}$ orbitals, respectively. Furthermore, several transitions connecting these two positive-parity bands indicate that some mixture of $\nu g_{7/2}$ and $\nu d_{5/2}$ single-particle configurations exist. The previously observed $11/2^-$ state at 2017 keV has been identified to be based on the $\nu h_{11/2}$ [31]. The excitation energy vs spin plots of the bands B1–B5 are shown in Fig. 6(a). The $\nu g_{7/2}$ (B1) and $\nu d_{5/2}$ (B2) bands exhibit similar trends. The excitation energy plot of band B5 lies ~450 keV above the $\nu g_{7/2}$ (B1) band, as expected for the associated γ-vibrational band in this mass region. The negative-parity $\nu h_{11/2}$ (B3) band lies ~1 MeV above the $\nu g_{7/2}$ (B1) band. Further, the $39/2^-$ (band B3) and $39/2^+$ (band B4) states have nearly the same excitation energies, 8183 and 8010 keV, respectively. The excitation energies for the bands B1–B4 along with various other observed states are also presented in Fig. 7 in the form of a rigid-rotor plot, where a rotating liquid drop energy reference has been subtracted. It indicates that the $21/2^+$ state at 2635 keV and $25/2^+$ state at 3546 keV are energetically more favored than the states in rotational bands. The $21/2^+$ state is fed by the 704.7-keV transition from the positive-parity band B4, and the 1379.2-keV transition from the negative-parity band B3, and the 911.4-keV transition from the $25/2^+$ state. It is worth noting that the 467.8-keV transition is assigned as $23/2^- \rightarrow 25/2^+$, that is, a transition to higher angular momentum state, which is unlikely for the usual deexcitation among the rotational states. However, it is probable in the case of population of a highly favored state [36]. The favored $21/2^+$ and $25/2^+$ states are expected to result from angular momentum coupling of the maximally aligned $g_{9/2}$ proton holes with the neutrons in the $g_{7/2}$ and $d_{5/2}$ orbitals, viz., the $[\pi(g_{9/2})^{-2} \otimes \nu d_{5/2}]_{21/2^+}$ and $[\pi(g_{9/2})^{-2} \otimes \nu d^3_{5/2}]_{25/2^+}$, respectively. Multifragmentation at the $39/2^-$ and $31/2^+$ states in bands B3 and B4, respectively, also indicates a loss of collectivity. These states are possibly the maximally aligned states with $[\pi(g_{9/2})^{-2} \otimes \nu(g_{7/2})^2 \otimes \nu h_{11/2}]_{39/2^-}$ and $[\pi(g_{9/2})^{-2} \otimes \nu g_{7/2} \otimes \nu(d_{5/2})^2]_{31/2^+}$ / $[\pi(g_{9/2})^{-4} \otimes \nu g_{7/2}]_{31/2^+}$ configurations, respectively.

A. Deformed Hartree-Fock and angular-momentum projection calculations

The observed level structures in the ^{99}Pd nucleus have been studied using the projected Hartree-Fock (PHF) technique. The formalism is discussed in Refs. [38–40]. In the deformed Hartree-Fock and angular-momentum projection (PHF) calculations, the HF equation is derived from the nuclear Hamiltonian consisting of the single-particle terms and the two-body interaction terms, and solved to get the single-particle orbits of nucleons. The model space considered is outside the inert spherical ^{80}Zr core with $Z = 40$ and $N = 40$. The surface δ (SD) interaction with strength $V_{pp} = V_{np} = V_{nn} = 0.36$ MeV is taken as the two-body residual interaction among 6 active protons and 13 active neutrons. This SD interaction strength is found to be consistent for this mass region [41,42]. The spherical single-particle orbits considered in the PHF calculations are $3s_{1/2}$, $2d_{3/2}$, $2d_{5/2}$, $1g_{7/2}$, $1f_{7/2}$, $1g_{9/2}$, and $1h_{11/2}$, with energies 2.129, 3.109, 0.0, 1.82, 7.596, −4.0484, and 3.066 MeV, respectively, for protons and $3s_{1/2}$, $2d_{3/2}$, $2d_{5/2}$, $1g_{7/2}$, $2f_{7/2}$, $1g_{9/2}$, and $1h_{11/2}$, with energies 2.008, 2.715, 0.0, 1.515, 7.763, −3.996, and 2.96 MeV, respectively, for neutrons. The HF iteration is

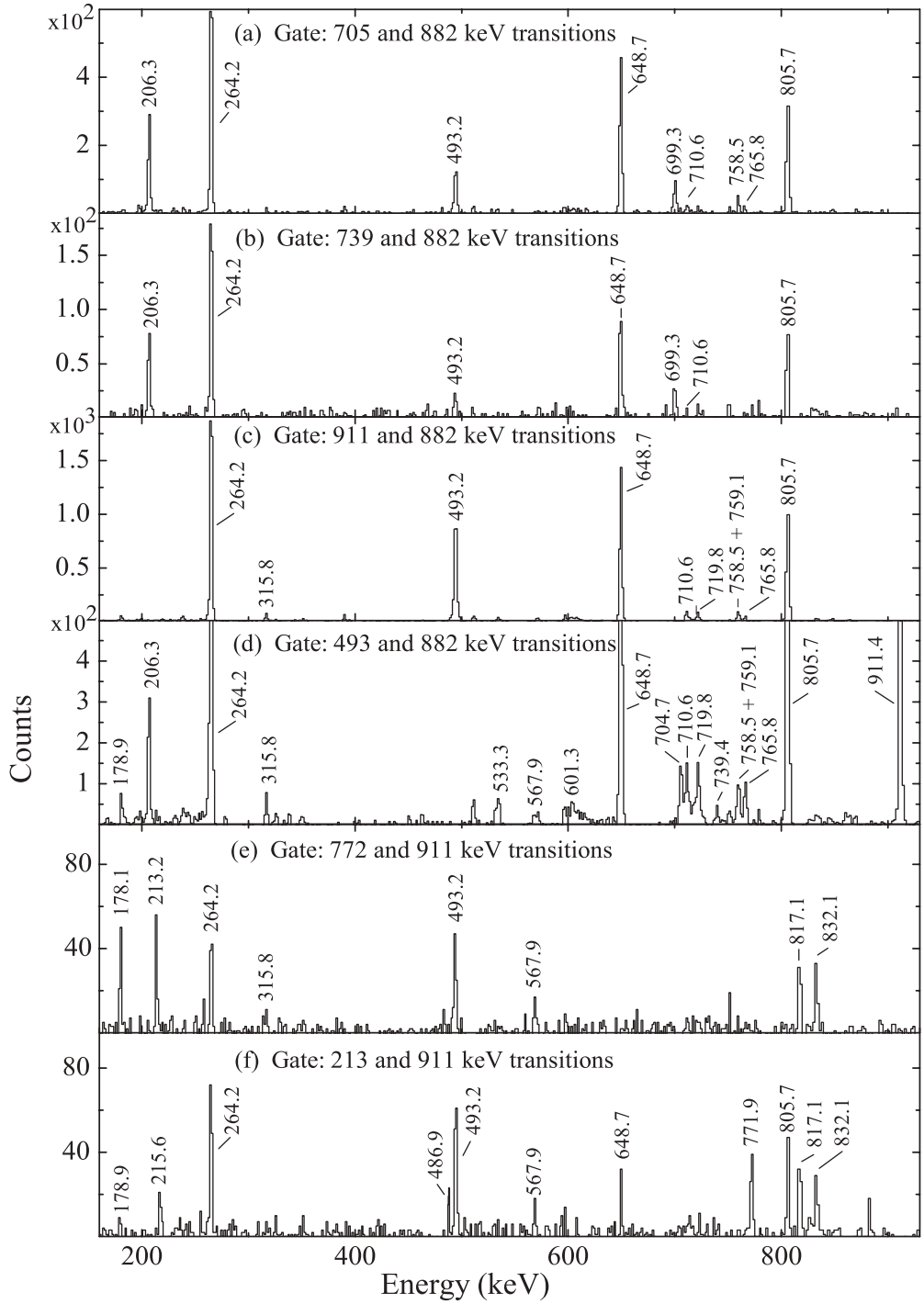

FIG. 5. γ-ray coincidence spectra with double gate on the (a) 705- and 882-keV transitions, (b) 739- and 882-keV transitions, (c) 911- and 882-keV transitions, (d) 493- and 882-keV transitions, (e) 772- and 911-keV transitions, and (f) 213- and 911-keV transitions. These spectra support placement of the unobserved 35-keV transition and its neighboring part in the level scheme of ^{99}Pd from the present work, as discussed in the text.

performed for both the prolate and the oblate deformations. Axial symmetry of the Hartree-Fock field is assumed in the calculations. Various one-, three-, and five-quasiparticle configurations were considered for angular momentum projection to understand the band structures. The details of calculations are given in Refs. [40,42]. The low-lying positive-parity states in ^{99}Pd have contributions from the $\pi g_{9/2}$, $\nu d_{5/2}$, and $\nu g_{7/2}$ orbitals, which are near the respective Fermi surfaces. The PHF calculations have been performed for various positive-parity configurations. The observed excitation energies of levels in ^{99}Pd are compared with the calculated ones for germane configurations for various bands in Figs. 6(a)–6(c).

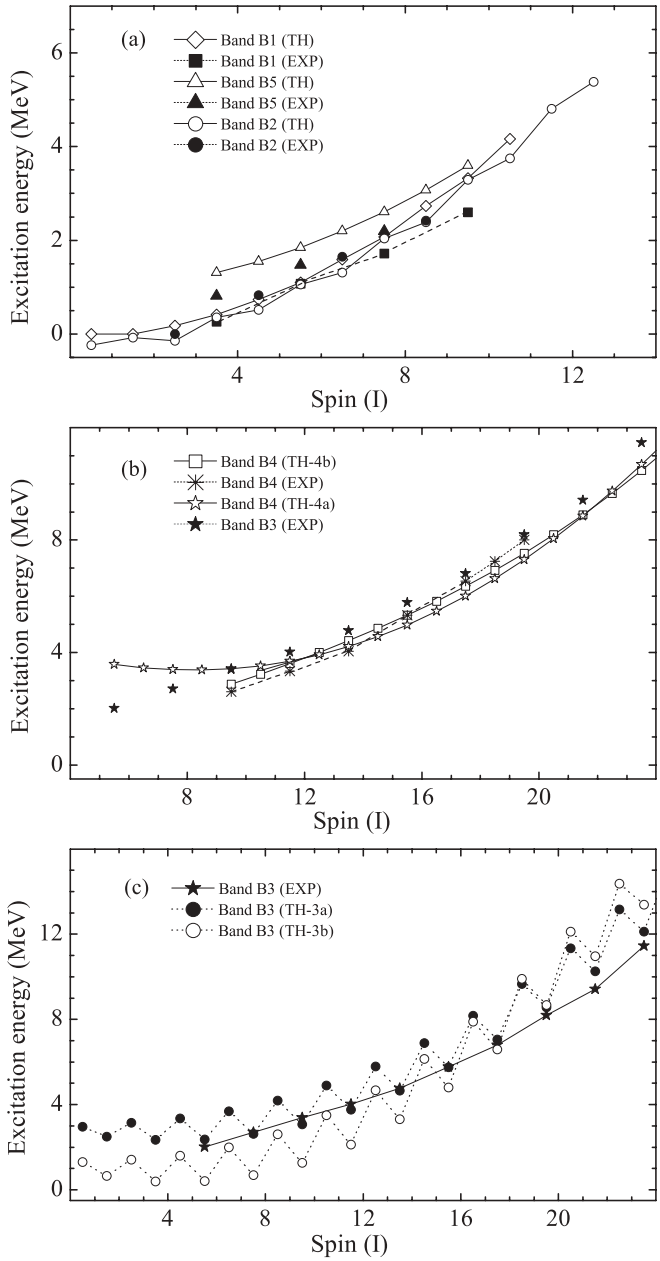

FIG. 6. Comparison of the observed energy levels of (a) bands B1, B2, and B5, and (b) and (c) bands B3 and B4 of ^{99}Pd with the PHF calculations.

The ground-state band B2 ($\nu d_{5/2}$) has bandhead at $I^\pi = 5/2^+$ and is reproduced for the configuration $\nu(g_{7/2})^2 \otimes \nu(d_{5/2}) \otimes \pi(g_{9/2})^6$, with $K = 1/2^+$. Band B1 with bandhead $I^\pi = 7/2^+$ has configuration $\nu(g_{7/2})^3 \otimes \pi(g_{9/2})^6$, with $K = 3/2^+$. The excited states in negative-parity band B3 lie well above the positive-parity band B4 [Fig. 6(b)]. Band B4 is closely reproduced for the two configurations: (a) $\pi(g_{9/2})^6 \otimes \nu(g_{7/2})^2 \otimes \nu(h_{11/2})^2 \otimes \nu(g_{9/2})^{-1}$, with $K = 5/2^+$ state, and (b) the other obtained by exciting one $g_{9/2}$ proton to $\Omega = 1/2^+$ ($g_{7/2}$) orbit, that is, $\pi(g_{9/2})^5 \otimes \pi(g_{7/2}) \otimes \nu(g_{7/2})^2 \otimes \nu(h_{11/2})^2 \otimes \nu(g_{9/2})^{-1}$ configuration, with $K = 19/2^+$. The corresponding plots are labeled as TH-4a and TH-4b, respectively, in Fig. 6(b). The lowest observed state in band B4 is $19/2^+$, which favors the

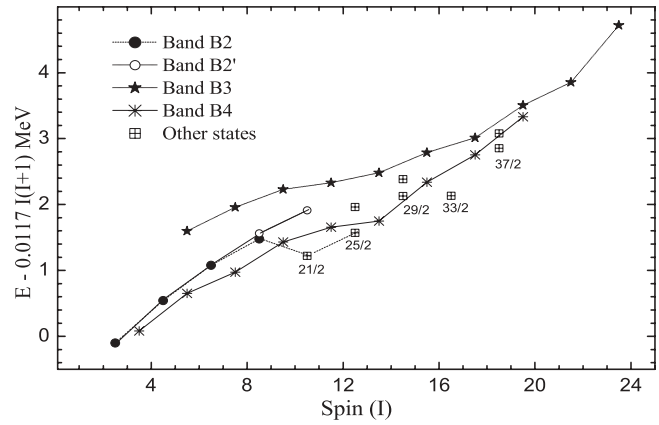

FIG. 7. Energies of various states in bands B1–B5 of ^{99}Pd relative to a rigid-rotor reference plotted as a function of spin.

configuration (b) with the p-h configuration in the neutron space and the core-excited configuration in the proton space.

The excited states in negative-parity band B3 are closely reproduced for two configurations: (a) the one resulting from mixing the $\pi(g_{9/2})^6 \otimes \nu(g_{9/2})^{10} \otimes \nu(g_{7/2})^2 \otimes \nu(h_{11/2})$ configurations, with $K = 1/2^-$ and $K = 3/2^-$, and (b) the other obtained by mixing the $\pi(g_{9/2})^6 \otimes \nu(g_{9/2})^8 \otimes \nu(g_{7/2})^2 \otimes \nu(d_{5/2})^2 \otimes \nu h_{11/2}$ configurations, with $K = 1/2^-$ and $K = 3/2^-$. Figure 6(c) shows comparison of the observed excitation energy of levels in band B3 with the calculated ones for the configurations (a) and (b), which are labeled as TH-3a and TH-3b, respectively. The favored component of TH-3a reproduces the only observed signature in band B3.

B. Octupole collectivity in ^{99}Pd

In the ^{99}Pd nucleus, the octupole-driving pair of neutron $h_{11/2}$ and $d_{5/2}$ orbits becomes accessible at low excitation energy. The signatures for octupole collectivity are interleaved positive-parity and negative-parity bands connected by enhanced $E1$ transitions. The $E1$ transitions from the levels of $\nu h_{11/2}$ band (B3) to $\nu d_{5/2}$ band (B2) have been observed in ^{99}Pd in the present work. The connecting $E1$ transitions are intense for the $15/2^-$, $19/2^-$, and $23/2^-$ states of $\nu h_{11/2}$ band, while the intraband $E2$ transitions dominate for the higher states in this band. The $27/2^-$ and $31/2^-$ states decay to the $25/2^+$ and $29/2^+$ states, respectively. The ratio of reduced transition probabilities for the $E1$ and $E2$ transitions are deduced using the relation

$$\frac{B(E1)}{B(E2)} = \frac{1}{1.3 \times 10^6} \frac{E_\gamma^5(E2)}{E_\gamma^3(E1)} \frac{I_\gamma(E1)}{I_\gamma(E2)} (\mathrm{fm}^{-2}),$$

where E_γ is in MeV. The branching ratios for the $E2$ and $E1$ transitions have been determined from the spectra obtained by gating the upper-lying $E2$ trasition. The extracted values of the $B(E1)/B(E2)$ ratios for $15/2^-$, $19/2^-$, $23/2^-$, $27/2^-$, and $31/2^-$ states are 1.2×10^{-7}, 2.0×10^{-7}, 0.3×10^{-7}, 0.1×10^{-7}, and 0.5×10^{-7}fm^{-2}, respectively. Using the quadrupole deformation, $\beta_2 \sim 0.15$, the resulting $B(E1)$ values are around 10^{-6} W.u., which indicate possible octupole correlations in the ^{99}Pd nucleus. These values are comparable to those

observed for the $E1$ transitions between the $\pi h_{11/2}$ and $\pi d_{5/2}$ bands in the mass A $\approx$ 120 region. Octupole collectivity has been observed in ^{117}Xe [20], ^{122,131}Cs [23,24], ^{141,143}Cs [26], ^{124,125}Ba [27], and ^{143,145}Ba [28], where the $\pi h_{11/2}$ and $\pi d_{5/2}$ orbitals ($\pi = -1$, $\Delta l = \Delta j = 3$) play an important role.

V. SUMMARY

The γ-ray spectroscopic investigation of the ^{99}Pd nucleus following population through the ^{75}As(^{28}Si, $p3n$) reaction at $E_{\rm lab}$ = 120 MeV and the deexcitations has resulted in substantial extension of band structures. The level scheme consisting of about five bands is established up to excitation energy $\sim$10 MeV and spin $\sim 25\hbar$ with the addition of about 60 new transitions. The $\nu g_{7/2}$ and $\nu d_{5/2}$ and vibrational band structures are identified at lower spins. The observed level structures in ^{99}Pd have been interpreted in the framework of a microscopic theory based on the deformed HF and angular momentum projection techniques. New bands have been interpreted as based on the $\pi(g_{9/2})^5 \otimes \pi(g_{7/2}) \otimes \nu(g_{7/2})^2 \otimes \nu(h_{11/2})^2 \otimes \nu(g_{9/2})^{-1}$ and $\pi(g_{9/2})^6 \otimes \nu(g_{9/2})^{10} \otimes \nu(g_{7/2})^2 \otimes \nu(h_{11/2})$ configurations. A few of these states may be interpreted as maximum spin aligned states with $[\pi(g_{9/2})^m \otimes \nu d^n_{5/2} \otimes \nu g^p_{7/2} \otimes \nu h_{11/2}]$ configurations. The new $E1$ transitions from $\nu h_{11/2}$ band to the $\nu d_{5/2}$ band in ^{99}Pd are observed. Weisskopf estimates for the $B(E1)$ values for the states of negative-parity band are around 10^{-6}, which is an indication of possible octupole correlations in the ^{99}Pd nucleus.

ACKNOWLEDGMENTS

Authors acknowledge the joint effort of IUAC, New Delhi, TIFR, Mumbai, and IUC-DAEF and SINP, Kolkata, in establishing the INGA clover array and thank the Department of Science and Technology, Government of India, for providing funds for the INGA project (Grant No. IR/S2/PF-03/2003-I). Thanks to the pelletron staff for smooth functioning of the accelerator. Financial support from UGC, New Delhi, under the Centre of Advanced Study Funds, and CSIR, New Delhi, is duly acknowledged.

[1] S. Lalkovski *et al.*, Phys. Rev. C **71**, 034318 (2005).
[2] V. P. Janzen *et al.*, Phys. Rev. Lett. **70**, 1065 (1993).
[3] W. Reviol *et al.*, Nucl. Phys. A **557**, 391C (1993).
[4] J. Gizon *et al.*, Z. Phys. A **345**, 335 (1993).
[5] A. Gadea, Phys. Rev. C **55**, R1 (1997).
[6] D. G. Jenkins *et al.*, Phys. Lett. B **428**, 23 (1998).
[7] P. Joshi, M. P. Carpenter, D. B. Fossan, T. Koike, E. S. Paul, G. Rainovski, K. Starosta, C. Vaman, and R. Wadsworth, Phys. Rev. Lett. **98**, 102501 (2007).
[8] J. Timár, C. Vaman, K. Starosta, D. B. Fossan, T. Koike, D. Sohler, I. Y. Lee, and A. O. Macchiavelli, Phys. Rev. C **73**, 011301(R) (2006).
[9] J. Timár *et al.*, Phys. Lett. B **598**, 178 (2004).
[10] P. Joshi *et al.*, Eur. Phys. J. A **24**, 23 (2005).
[11] K. Higashiyama and N. Yoshinaga, Prog. Theor. Phys. **120**, 525 (2008).
[12] J. Cederkäll *et al.*, Eur. Phys. J. A **1**, 7 (1998).
[13] D. Sohler *et al.*, Eur. Phys. J. A **16**, 171 (2003).
[14] J. Cederkäll *et al.*, Z. Phys. A **359**, 227 (1997).
[15] J. Gizon *et al.*, Phys. Lett. B **410**, 95 (1997).
[16] B. M. Nyakó *et al.*, Phys. Rev. C **60**, 024307 (1999).
[17] E. S. Paul, D. B. Fossan, J. M. Sears, and I. Thorslund, Phys. Rev. C **52**, 2984 (1995).
[18] K. Starosta, T. Koike, C. J. Chiara, D. B. Fossan, and D. R. LaFosse, Nucl. Phys. A **682**, 375c (2001).
[19] E. S. Paul *et al.*, Nucl. Phys. A **644**, 3 (1998).
[20] Z. Liu *et al.*, Eur. Phys. J. A **1**, 125 (1998).
[21] W. Urban *et al.*, Eur. Phys. J. A **16**, 303 (2003).
[22] G. de Angelis *et al.*, Phys. Lett. B **535**, 93 (2002).
[23] R. Kumar *et al.*, Phys. Rev. C **72**, 044319 (2005).
[24] S. Sihotra *et al.*, Phys. Rev. C **78**, 034313 (2008).
[25] S. H. Liu, J. H. Hamilton, A. V. Ramayya, Y. X. Luo, J. O. Rasmussen, J. K. Hwang, S. J. Zhu, W. C. Ma, A. V. Daniel, and G. M. Ter-Akopian, Phys. Rev. C **81**, 057304 (2010).
[26] W. Urban, T. Rzaca-Urban, J. L. Durell, W. R. Phillips, A. G. Smith, B. J. Varley, N. Schulz, and I. Ahmad, Phys. Rev. C **69**, 017305 (2004).
[27] P. Mason *et al.*, Phys. Rev. C **72**, 064315 (2005).
[28] S. J. Zhu *et al.*, Phys. Rev. C **60**, 051304(R) (1999).
[29] M. Huyse, K. Corneils, G. Lhersonneau, J. Verplancke, W. B. Walters, K. Heyde, P. Van Isacker, M. Waroquier, G. Wenes, and H. Vinex, Nucl. Phys. A **352**, 247 (1981).
[30] W. F. Piel Jr. and G. Scharff-Goldhaber, Phys. Rev. C **15**, 287 (1977).
[31] J. Dubuc, G. Kajrys, P. Lariviére, N. Nadon, S. Pilotte, S. Monaro, and J. C. Waddington, Phys. Rev. C **37**, 1932 (1988).
[32] S. Muralithar *et al.*, Nucl. Instrum. Methods A **622**, 281 (2010), and references therein.
[33] D. C. Radford, Nucl. Instrum. Methods A **361**, 306 (1995).
[34] D. Negi *et al.*, Phys. Rev. C **81**, 054322 (2010).
[35] R. Palit, H. C. Jain, P. K. Joshi, S. Nagaraj, B. V. T. Rao, S. N. Chintalapudi, and S. S. Ghugre, Pramana **54**, 347 (2000).
[36] W. F. Piel Jr., D. B. Fossan, R. Ma, E. S. Paul, N. Xu, and J. B. McGrory, Phys. Rev. C **41**, 1223 (1990).
[37] R. Popli, F. A. Rickey, and P. C. Simms, Phys. Rev. C **22**, 1121 (1980).
[38] G. Ripka, in *Advances in Nuclear Physics*, edited by M. Baranger and E. Vogt (Plenum, New York, 1966), Vol. 1.
[39] R. E. Peierls and Y. Yoccoz, Proc. Phys. Soc. A **70**, 381 (1957).
[40] C. R. Praharaj, J. Phys. G **14**, 843 (1988).
[41] A. Faessler, P. Plastino, and S. A. Moszkowski, Phys. Rev. **156**, 1064 (1967).
[42] Z. Naik and C. R. Praharaj, Phys. Rev. C **67**, 054318 (2003).